Journal of
**Applied Crystallography**
ISSN 0021-8898

Received 14 August 2006
Accepted 15 December 2006

# Fracture of poly(vinylidene fluoride): a combined synchrotron and laboratory *in-situ* X-ray scattering study

**Günther A. Maier,[a]* Gernot M. Wallner,[b] Reinhold W. Lang,[b] Jozef Keckes,[a] Heinz Amenitsch[c] and Peter Fratzl[d]**

[a]Material Center Leoben, Erich Schmid Institute of Material Science and Department of Material Physics, University of Leoben, Leoben, Austria, [b]Polymer Competence Center Leoben and Institute of Materials Science and Testing of Plastics, University of Leoben, Leoben, Austria, [c]Institute of Biophysics and Nanosystems Research, Austrian Academy of Sciences, Graz, Austria, and [d]Max Planck Institute of Colloids and Interfaces, Department of Biomaterials, 14424 Potsdam, Germany. Correspondence e-mail: guenther.maier@unileoben.ac.at

Semi-crystalline polymers show a complex fracture mechanism, which is controlled by the micro-mechanisms associated with formation and breakdown of a plastic deformation region. Such regions develop at notches, cracks or other stress-raising defects. In the present paper, we use time-resolved synchrotron X-ray scattering techniques during the deformation process in poly(vinylidene fluoride) to study the plastic zone formation and fracture processes at different strain rates. This gives new insight into the micro-mechanisms of cavitation, lamellae separation and fibril formation in this particular material.



## 1. Introduction

The hierarchical structure of semi-crystalline polymers, such as poly(vinylidene fluoride) (PVDF), leads to complex fracture mechanisms. While 'hard' crystalline regions can act as stress concentrators, the 'soft' amorphous material in-between the lamellae allows the material to extend (Ward & Sweeny, 2000). In many semi-crystalline polymers, the two main deformation mechanisms, crazing and shear yielding, were found to occur simultaneously when irreversible plastic deformation was applied (Ward & Sweeny, 2000). At stress-raising defects, like notches and cracks, numerous deformation mechanisms are related to the formation of shear bands or crazes. In a previous study, we investigated the structural details around a crack tip in PVDF using scanning scattering methods on *post mortem* samples (Maier *et al.*, 2005). In PVDF (Lovinger, 1980), the crystalline phase undergoes a phase transition when highly oriented forces are applied, accompanied by the formation of thin fibrils. However, with *post mortem* samples it is not possible to gain information about kinetics and detailed failure mechanisms. To gain information about dynamical deformation processes in polymeric materials many *in situ* X-ray scattering studies were performed during the last decade (Keckes *et al.*, 2003; Butler *et al.*, 1995; Wu *et al.*, 2000; Legrand *et al.*, 1986; Fakirov *et al.*, 2001). We used this technique for investigating the dynamical processes occurring ahead of a crack tip in PVDF, which is in our opinion a very interesting model material for polymers. We performed fast tensile experiments at a synchrotron as well as slow tensile tests using laboratory sources, gaining new insights about the kinetics of deformation processes in PVDF.

## 2. Experimental

### 2.1. Material and specimen preparation

From 200 µm-thick $\alpha$-PVDF (Maier *et al.*, 2005) films rectangular samples having a width of 10 mm and a length of 40 mm were cut parallel to the extrusion direction. The films were razor-notched to obtain double-notched tensile specimens (DENT), with an unbroken ligament length of 6 mm and symmetrical initial notches. The principles of DENT sample geometry and detailed analysis of the mechanical properties of the used PVDF are described in Wallner *et al.* (2006).

### 2.2. *In situ* X-ray scattering experiments

Synchrotron X-ray measurements were performed at the Austrian SAXS beamline at Elettra Trieste (Italy) (Amenitsch *et al.*, 1997), using an imaging intensified two-dimensional (2D) charge-coupled device detector (Photonic Sciences, Robertsbridge, UK). The size of the beam was approximately 1 × 1 mm with a wavelength $\lambda$ of 0.154 nm. The measuring times were 2 s for wide-angle X-ray diffraction (WAXD) and 0.3 s for small-angle X-ray scattering (SAXS) measurements. Slow fracture experiments were performed in the laboratory using a NanoSTAR SAXS system (Bruker AXS, Karlsruhe, Germany) with a sealed-tube Cu X-ray source and WAXD system with X-rays from a rotating Cu anode (GADDS, Bruker AXS, Karlsruhe, Germany). All *in situ* tensile experiments were performed at room temperature of approximately 298 K in an in-house constructed tensile tester (Keckes *et al.*, 2003). The PVDF films were fixed between clamps and the free length of the material was 20 mm with the notches in the center. The exact position of the notch was determined using radiography. The beam penetrated the sample 2 mm ahead of the notch. To keep a constant measuring position on the sample, the tensile tester was moved against the drawing direction with half of the displacement rate. WAXD patterns were collected first, SAXS measurements were performed using a new set of samples. For slow tensile experiments, samples were strained with 0.01 mm $s^{-1}$, the extension was stopped approximately every 0.1 mm and the sample was allowed to relax prior measurement. The measurement time was 300 s for SAXS and 200 s for WAXD. For data evaluations all patterns were corrected for background scatter. Primary data treatment and integrations were performed using the

*FIT2D* software for synchrotron data and the *SAXS NT* and *GADDS NT* software for the laboratory experiments.

### 2.3. Small-angle X-ray scattering data analysis

To determine morphological parameters, SAXS patterns $I(q, \psi)$ were averaged in arcs with respect to $\psi = -15$ to $15^\circ$ (parallel to the drawing direction) and $\psi = 75$ to $105^\circ$ (orthogonal to the drawing direction). The drawing direction was defined as $\psi = 0^\circ$ and $\psi$ denotes the azimuth angle. The modulus of the scattering vector $q$ is defined as $q = 4\pi(\sin\theta)/\lambda$ where $\lambda$ is the wavelength of the radiation used and $\theta$ is half of the scattering angle $2\theta$. The scattering curves were analyzed applying a one-dimensional correlation function method (Strobl & Schneider, 1980) to calculate the long period and the thickness of the crystal lamellae. This allowed for determination of the extension of amorphous phase with respect to the drawing direction. Oriented SAXS patterns were reduced by averaging within arcs from $\psi = -15$ to $15^\circ$, where the main orientation was defined as $\psi = 0^\circ$. For fibril-like structures, a cross-sectional radius of gyration $R_{gc}$ was derived using an exponential law, modified from the usual Guinier law (Guinier & Fournet, 1955; Fratzl, 1997; Maier *et al.*, 2005). To calculate the invariant, the scattering patterns $I(q, \psi)$ were spherically averaged over a cylinder with the drawing direction being the cylinder axis, yielding the $I'(q, \psi)$ pattern. The $I'(q, \psi)$ patterns were radially averaged with respect to $\psi$, yielding the $I'(q)$ scattering curves. This curves were extrapolated to high $q$ values using Porod's law (Porod, 1951) and extrapolated to $q = 0$ by linear extrapolation of the measured intensities at low $q$ values. The invariant ($I$) is given by $I = \int q^2 I'(q)\, dq$ between the borders 0 and $q_{max}$. $q_{max}$ is the highest $q$ value from the extrapolation. The invariant is defined as $I = 2\pi^2 V \eta^2$, with $V$ being the sample volume depending on the beam size and the material thickness and $\eta^2$ is the mean electron density contrast between the scattering objects.

### 2.4. Wide-angle X-ray diffraction data analysis

For evaluation, two-dimensional scattering patterns were recorded at the synchrotron and were reduced by averaging within arcs of $\psi =$ 70–140° with respect to $\psi$. $\psi = 0^\circ$ indicated the drawing direction. The $\beta/\alpha$-phase ratio was estimated according to Maier *et al.* (2005).

## 3. Results

A typical force–extension curve of the investigated $\alpha$-PVDF film is shown in Fig. 1 along with photographic pictures illustrating the double-notched region of the deformed specimen for various deformation stages. In the first region of the force–extension diagram, plastic deformation zones with a white appearance developed at both razor notch tips. As the load was increased to the maximum point, the plastic deformation zones with a white appearance grew from both notch tips, approached one another and merged, leading to a state of full ligament yielding. Furthermore, a second type of plastic deformation zone with a transparent-white appearance developed at both razor notch tips. The second plastic deformation zones also approached one another and joined immediately after the load maximum, causing the load deformation instability. Upon further deformation, significant crack growth from the meanwhile blunted razor notch roots occurred in the unbroken, transparent-white midrib region surrounded by an outer white plastic zone region. The process of crack growth continued until ultimate failure and specimen separation occurred. The measuring position was fixed 2 mm ahead of one of the crack tips. As a consequence of deformation, a sequence of events was studied at this measuring position (Fig. 1).

First, the position was outside the white zones, which start to form at the notch tips (Fig. 1, I). Later, the position was within the growing white zone (Fig. 1, II), which was followed by the second, transparent deformation zone (Fig. 1, III). Finally, the crack tip region itself was studied (Fig. 1, IV). Slow experiments were performed in steps, as described in the experimental part of this work. The relaxation led to a reduction of the maximum force at the yield point, but final fracture occurred at nearly the same extension. The results from the synchrotron experiments are shown in Fig. 2. Small-angle scattering patterns (a), (b) and (c) were taken at different extension levels of the sample.

Pattern (a) showed a ring, arising from the isotropic and spherulitic $\alpha$-PVDF films used for this study. After an elongation of approximately 2 mm, the isotropic lamellae scatter had disappeared completely and changed to an elongated streak orthogonal to the drawing direction and a second scattering signal oriented parallel to the tensile direction (b). After an extension of approximately 3 mm, the second signal had disappeared and the streak, orthogonal to the strain axis, became sharper. Fig. 2(d) shows the invariant ($I$) plotted against the extension. Fig. 2(e) shows the corresponding force–extension curve. Like the force–extension curve, the invariant–extension curve could be divided into four different regions. Region (I) is the deformation region with no changes in the overall electron-density differences in the material, with a non-gradient linear behavior of the invariant curve. In region II, just after the maximum load point, the invariant increased strongly. A change in the electron-density distribution had occurred. The raise in the invariant was caused by the formation of cavities and the reorientation from spherulitic to a shish-kebab-like lamellae structure. In region III, a plateau occurred in the invariant *versus* extension curve, indicating that there were no ongoing changes in the electron-density distribution. At the end of zone III and the beginning of zone IV, the invariant suddenly began to decrease in a linear way. At the same time, the $\alpha$-to-$\beta$ PVDF phase transition, revealed by the WAXD pattern, occurred (f). In Fig. 2(f) the long period ($L$) and the thickness ($d$) of the lamellae are also plotted against the extension. In the drawing direction, the lamellae were separated from each other by stretching the amorphous zone in-between the crystals. This is indicated by the fact that the long period increases strongly while the lamellae thickness stayed nearly constant. No changes in morpholo-

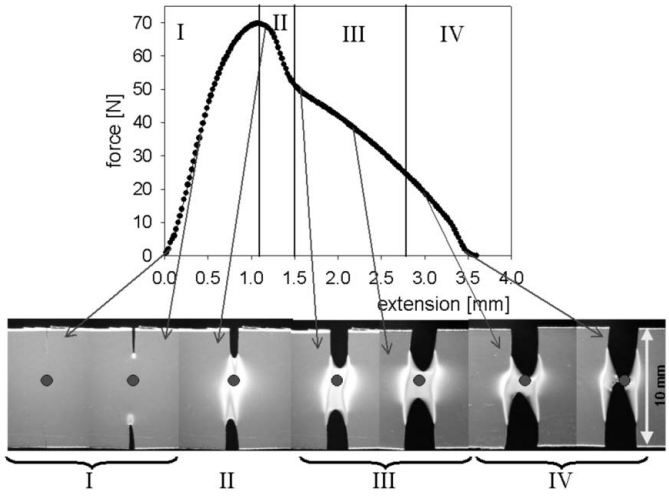


**Figure 1**
Typical load–extension curve of PVDF DENT samples and the corresponding photographic pictures taken at different extension levels. Drawn points indicate the size and position of the X-ray beam on the sample.

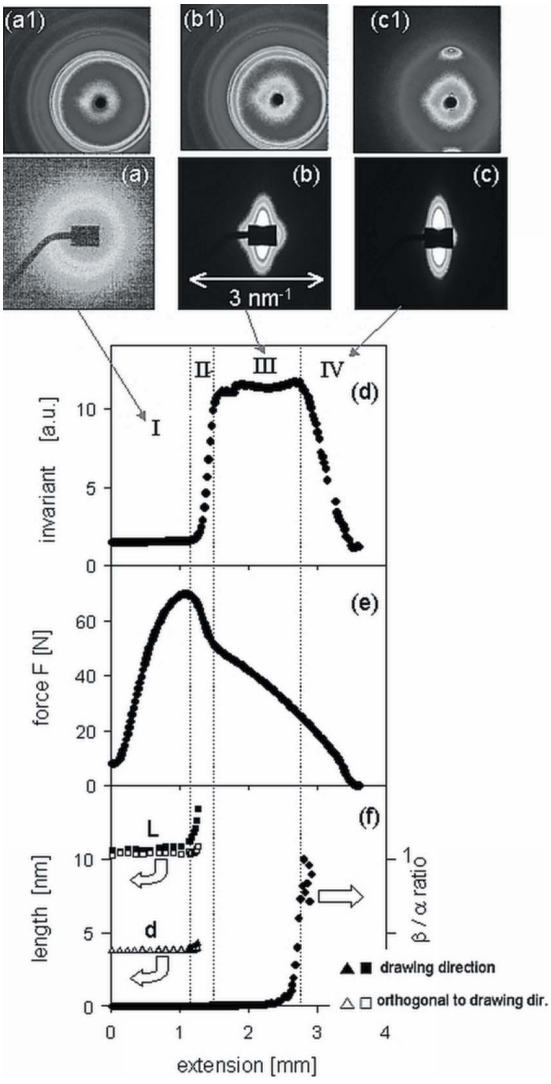


**Figure 2**
Synchrotron experiments: Selected SAXS (a), (b) , (c) and WAXD (a1), (b1), (c1) patterns recorded at the same extension. The SAXS $q$ range is indicated in the figure. The invariant (d), force (e) and $\beta/\alpha$ ratio are plotted against the extension. The long period ($L$) and lamellar thickness ($d$) (f) were determined from the scattering curves which were gained by reduction of the two-dimensional patterns in arcs.

gical parameters occurred orthogonal to the drawing direction during the experiments.

Fig. 3 highlights the correlation of the load and SAXS invariant as a function of extension in both types of experiments, slow and fast, by showing the derivative (diff) of these curves. For better comparison between different experiments, the extension was normalized to its maximum value. The invariant stayed constant until an extension of 32 and 29%, for fast and slow tensile experiments, respectively. This corresponded to the load maxima. After this point, a strong increase in the invariant occurred simultaneously with a load drop in the force–extension curve. Just after the point of inflexion in the load–extension curve at 37 and 35%, the invariant reached its maximum value and stayed constant until approximately 74% extension.

At this extension the $\alpha$-to-$\beta$ phase transition occurred in the fast experiments, while the phase transition at low deformation rates occurred at 40 to 45% extension. At these extensions, the oriented $\alpha$-shish-kebab-like structure transformed to $\beta$-PVDF fibrils, with diameters depending on the displacement rate: 14.4 $\pm$ 1 nm and

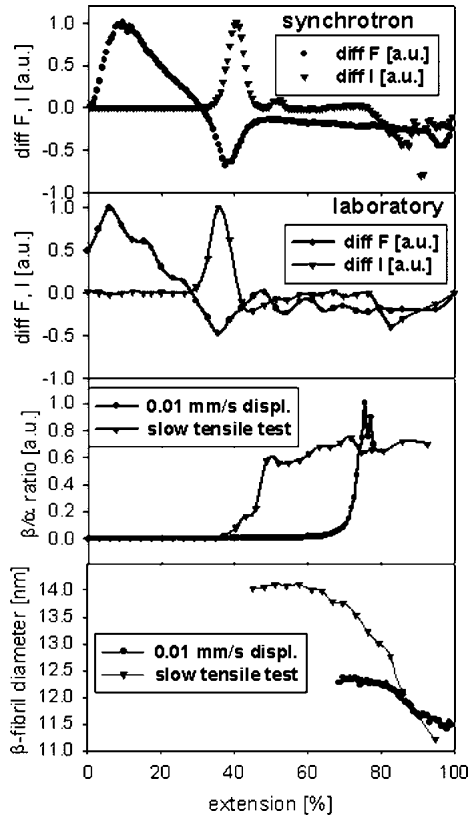


**Figure 3**
Comparison of the results from synchrotron experiments (0.01 mm s$^{-1}$ displacement) and the laboratory experiments (low tensile experiments). To highlight the main characteristics, the first derivatives from the curves were calculated and plotted against the normalized extension. The normalized extension (NE) was calculated by NE = (extension/ultimate extension) $\times$ 100. The $\beta/\alpha$ ratio and $\beta$-fibril diameters are also plotted against the extension.

12.5 $\pm$ 1 nm for the laboratory and synchrotron experiments, respectively. Continued extension led to thinning of the fibrils to a diameter of 11.5 $\pm$ 1 nm for both experiments, as shown in Fig. 3.

## 4. Discussion

In a previous study, we investigated the structural details of a deformation zone in PVDF after unloading the sample. It was found that the crack process zone was mainly formed by thin $\beta$-PVDF fibers. Using *in situ* techniques, we now had the possibility to clarify the kinetics of the formation of the plastic zone in context with deformation rate. At the beginning of deformation mainly elastic deformation occurred, caused by the extension of the amorphous phase parallel to the applied force. At the onset of plastic deformation, cavities oriented orthogonal to the tensile axis (Castagnet *et al.*, 2000) were formed. This allowed for stress reduction in the amorphous phase and continued lamellae separation. Because of viscoelastic relaxation in the material, no lamellae separation occurred at low deformation rates. Reorientation of the spherulitic material to a fibrous, shish-kebab-like morphology followed at continued extension. Interestingly, the orientation of lamellae crystals, as revealed by WAXD, was not affected by the reorientation (see Fig. 2). This fact can be explained assuming a shear-rotation mechanism associated with lamellae fragmentation (Butler *et al.*, 1995) for the reorientation process. Upon further deformation the fibrils were transformed to $\beta$-PVDF. This phase transition was effected by the strain rate. When the

extension rate was sufficiently slow, phase transformation occurred earlier as at higher extension rates. This indicated that the phase transition was both time and strain controlled.

## 5. Conclusion

In this paper, we presented an *in situ* X-ray measurement of fracture propagation in PVDF. The measurements of fast tensile experiments were taken at a synchrotron beamline, while slow tensile experiments were performed in the laboratory. Samples of the DENT type were used because they provide a well defined plastic zone and a predictable crack propagation path. Using the *in situ* X-ray scattering techniques, we have been able to characterize elastic deformations as well as the formation of plastic zones, including cavity formation, fibrillation and phase transitions prior to final fracture. Interestingly, the formation of oriented $\alpha$-PVDF shish-kebab structures was not accompanied with a change in the overall orientation of lamellae crystals. Therefore we were able to define a deformation mechanism being mainly related to lamellae shear with simultaneous rotation. Upon ongoing loading, the $\alpha$-PVDF shish kebab transformed to $\beta$-PVDF fibrils. These fibrils had an initial diameter depending on the deformation rate and crack propagation occurred by thinning and fracture of these fibrils.

The research work in the Materials Center Leoben (MCL) and in the Polymer Competence Center Leoben (PCCL) was supported by the Kplus program of the Austrian Ministry of Traffic, Innovation and Technology and by Bruker AXS, Karlsruhe, Germany. The PCCL is also supported by the State Governments of Styria and Upper Austria.

## References

Amenitsch, H., Bernstorff, S., Kriechbaum, M., Lombardo, D., Mio, H., Rappolt, M. & Laggner, P. (1997). *J. Appl. Cryst.* **30**, 872–876.
Butler, M. F., Donald, A. M., Bras, W., Mant, G. R., Derbyshire, G. E. & Ryan, A. J. (1995). *Macromolecules*, **28**, 6283–6393.
Castagnet, S., Girault, S., Gacougnolle, J. L. & Dang, P. (2000). *Polymer*, **41**, 7523–7530.
Fakirov, S., Samokovliyski, O., Stribeck, N., Apostolov, A. A., Denchev, Z., Sapoundjieva, D., Evstatiev, M. & Stamm, M. (2001). *Macromolecules*, **34**, 3314–3317.
Fratzl, P. (1997). *PSI - Proceedings*, **97–01**, 162–174.
Guinier, A. & Fournet, G. (1955). *Small-Angle Scattering of X-rays*. New York: John Wiley.
Keckes, J., Burgert, I., Fruhmann, K., Muller, M., Kolln, K., Hamilton, M., Burghammer, M., Roth, S., Stanzl-Tschegg, S. & Fratzl, P. (2003). *Nature Mater.* **2**, 810–814.
Legrand, J. F., Delzenne, P. & Lajzerowics, J. (1986). *IEEE Trans. Electr. Insul.* **21**, 551–554.
Lovinger, A. J. (1980). *J. Polym. Sci. B Polym. Phys.* **18**, 793–809.
Maier, G., Wallner, G., Lang, R. & Fratzl, P. (2005). *Macromolecules*, **38**, 6099–6105.
Porod, G. (1951). *Kolloid Z.*, **124**, 83–114.
Strobl, G. R. & Schneider, M. J. (1980). *J. Polym. Sci. B Polym. Phys.* **18**, 1343–1359.
Wallner, G. M., Major, Z., Maier, G. A. & Lang, R. W. (2006). *Adv. Eng. Mater.* **8**, 1140–1145.
Ward, I. M. & Sweeny, J. (2000). *An Introduction to the Mechanical Properties of Solid Polymers*. London: John Wiley and Sons Ltd.
Wu, J., Schulz, J. M., Yeh, F., Hsiao, B. S. & Chu, B. (2000). *Macromolecules*, **33**, 1765–1777.